http://dx.doi.org/10.21577/0103-5053.20190057

J. Braz. Chem. Soc., Vol. 30, No. 8, 1587-1598, 2019
Printed in Brazil - ©2019 Sociedade Brasileira de Química

Article

Droplet Size Distribution in Water-Crude Oil Emulsions by Low-Field NMR

Vinícius G. Morgan,[a] Cristina M. S. Sad,[a] Andre F. Constantino,[a] Rodrigo B. V. Azeredo,[b] Valdemar Lacerda Jr.,[a] Eustáquio V. R. Castro[a] and Lúcio L. Barbosa[c]*

[a]*Laboratório de Pesquisa e Desenvolvimento de Metodologias Para Análise de Petróleos (LabPetro), Universidade Federal do Espírito Santo (UFES), 29075-910 Vitória-ES, Brazil*

[b]*Instituto de Química, Universidade Federal Fluminense (UFF), 24020-290 Niterói-RJ, Brazil*

[c]*Departamento de Engenharia de Petróleo, Universidade Federal de São Paulo (Unifesp), 11030-400 Santos-SP, Brazil*

This paper reports the droplet size distribution (DSD) measurements in 28 W/O (water/oil) crude oil emulsions prepared with two Brazilian oils (medium and heavy) under different shear conditions using both 10 g L^{-1} NaCl solution and water production by low field nuclear magnetic resonance (NMR, 2.2 MHz). The PFGSTE (pulsed-field gradient-stimulated echo) pulse sequence applied was able to separate the crude oil emulsion signal for both medium and heavy oil even for low dispersed phase content (1.51 wt.%) and took into account only the aqueous phase signal. All emulsions exhibited an average diameter smaller than 5.5 μm because of the severe shear conditions. Despite the difficult processing of the S24 (6.48 wt.%) emulsion signal, good agreement was achieved between low field NMR and low-angle laser light scattering (LALLS) results. Finally, the paramagnetic ions in the water production did not affect the NMR measurements, demonstrating its applicability for analyzing real emulsions.

Keywords: crude oil emulsions, drop size distribution, low field NMR

Introduction

Water/oil (W/O) emulsion is very common in the oil industry, formed by contact between the fluids and turbulent conditions during oil production.[1] Natural surfactants (resins, naphthenic acids and asphaltenes), as well as solid particles, can stabilize the droplets,[2,3] which make phase separation difficult. The emulsions present cause numerous problems in operations, such as increase in viscosity and consequently production costs,[4,5] equipment corrosion and poisoning of catalyst used in refinery, among others.[6]

An important property of this system is the droplet size distribution (DSD) because it influences emulsion viscosity and stability[7-10] and it can be used to classify emulsions.[11,12] Each treatment method functions within a range of droplet size, so DSD can indicate the best method,[7] such as gravitational separation and advanced process, among others. Additionally, control, monitoring and correcting of equipment dimension can be carried out by using DSD data, contributing to transportation and treatment cost reduction of oil.

The DSD measurements are generally performed by optical methods, like laser scattering[9-11] and microscopy.[13] However, dilution steps, chemical costs, crude oil emulsion opacity and solid particles can make measurements difficult, leading to errors. On the other hand, nuclear magnetic resonance (NMR) is non-destructible, not restricted to a few droplets of the system, the opacity of the emulsion do not interfere in the analysis and not require dilution steps or chemicals.[2,7,14,15] Furthermore, the NMR technique is well established in crude oil studies, which provides permeability and porosity of rocks,[16-19] oil viscosity,[20-22] oil fraction physicochemical properties,[23] water content[24] and DSD[4,25-29] of emulsions.

NMR DSD measurements are generally used with respect to the restricted diffusion theory, which states that droplet size limits molecule diffusion, making the restricted diffusion coefficient (D_r) smaller than the free diffusion coefficient (D_f), which can be quantified by a pulsed magnetic field gradient similar to that proposed by Tanner.[30]

*e-mail: vljuniorqui@gmail.com

This theory was proposed by Murday and Cotts,[31] who extended the analysis developed by Neuman[32] to measure spherical particles radius using pulsed-field gradient. Later, Packer and Rees[33] proposed the use of the lognormal distribution to determine emulsion droplet size distribution, allowing for its wide use in DSD measurements.[34]

Following initial studies, many improvements to DSD measurements by NMR were introduced. Hollingsworth *et al.*[14] developed a diffusion train pulse sequence (DIFFTRAIN), which applies a single excitation pulse to produce successive stimulated echoes and recovery of the magnetization for each echo. The pulse sequence was able to measure DSD between 3 and 10 s, thereby opening up the possibility of evaluating non-equilibrium emulsions. Ambrosone *et al.*[34] applied the pulsed-field gradient-spin echo (PFGSE)[35] with generator functions to produce DSD without assuming distribution form. The generator functions method can work with anomalous or highly asymmetric distributions, providing good results. Hollingsworth and Johns[36] also demonstrated that the regularization technique can provide DSD without assuming the distribution form, and the generalized cross validation method is the most reliable when the error cannot be estimated.

Despite these advances, there are still just a few works that report analysis of crude oil emulsions by NMR. In general, the magnetic field are relatively superior in comparison to the field used in this work (0.052 T). The volumetric fractions and shear condition variation effects in DSD investigations are little explored in the literature as well. Furthermore, authors have often used a NaCl solution as the dispersed phase, disregarding the paramagnetic ion presence in the production water, responsible for relaxing the NMR signal.

Aichele *et al.*[27] developed the pulsed-field gradient with diffusion editing (PFG-DE) and demonstrated it to be more capable of solving bimodal distributions. They measured the DSD emulsions in two light oils (0.85 and 0.81 g mL^{-1}) and obtained diameters ranging from 19 to 59 μm. Despite robust agreement between PFG and PFG-DE, the experimental time was very high (7 h), making it unfeasible for routine use. In addition, all emulsions had a 20% dispersed phase. Opedal *et al.*[28] utilized a 23 MHz spectrometer to evaluate W/O emulsions in three heavy oils. The comparison with optical microscopy exhibited similarity between results, with drops ranging from 1 to 2 μm. However, they used pure water as the dispersed phase, disregarding the paramagnetic ions found in the production water. Fridjonsson *et al.*[37] optimized DSD measurements in crude oil emulsions applying a pulse sequence, as in the case of this article, based on continuous phase signal elimination by means of inversion time (T_{inv}) with 20 MHz spectrometer. The emulsions had 5, 10 and 20% of water dispersed phase and the results showed correct signal oil elimination by T_{inv} and good agreement with chemical shift measurements.

The present work describes the use of a 2.2 MHz NMR spectrometer to analyze the DSD crude oil emulsions in different shear conditions using medium and heavy oil with varying dispersed phase content. Emulsions were prepared with production water aiming to produce real emulsions. Finally, the results of droplet size distribution and difficulties and advantages of NMR experiment are discussed.

Experimental

Background theory

The majority measurements of DSD by NMR are based on the molecular diffusion of spins using magnetic field-gradient pulses. For DSD measurement, the PFGSTE (pulsed-field gradient-stimulated echo) technique (Figure 1b) is more advantageous than the PFGSE technique (Figure 1a) because it permits to use large Δ (time between the two gradiente pulses) values, allowing measure larger drops.[38]

In pulsed-field gradient techniques, the first gradient pulse makes the spins spatially dependent on the position and marks their initial position, thereby demarcating with a "magnetic label". A second gradient pulse reads the "magnetic label" and observes the spin displacement during Δ time.[39] This procedure is performed assuming that the second pulsed magnetic field gradient can completely

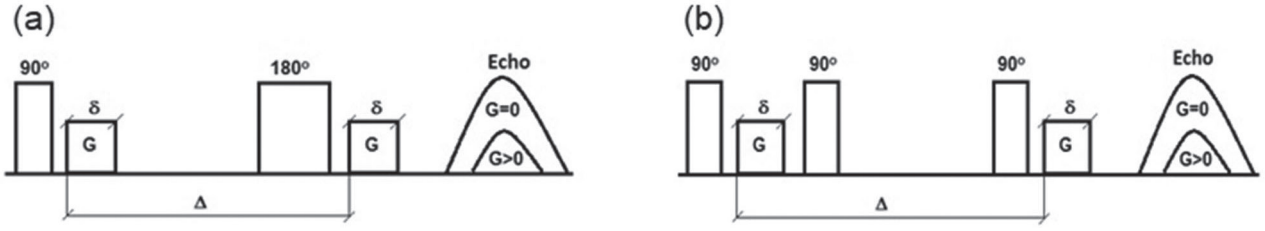

Figure 1. Pulsed-field gradient sequences: (a) PFGSE[30] and (b) PFGSTE[36] sequences. In PFGSTE, two 90° pulses are applied instead of the 180° pulse of the PFGSE sequence.

cancel out the phase coherent loss effect imposed by the first pulse, so the remaining lag is attributed to the diffusion of spins.[35] For a free moving liquid, when utilizing PFGSE, the signal decay is given by:

$$\frac{I}{I_0} = \exp\left[-D\left(\Delta - \delta/3\right)(\gamma\delta g)^2\right] \quad (1)$$

where I and I_0 are the signal intensities in the presence and absence of gradient pulses, respectively, D is the coefficient of diffusion, γ is the nuclear magnetogyric ratio, g is the gradient pulse intensity, δ is the duration time of this pulse.

However, when molecules move inside small compartments, there is an internal magnetic field distribution that varies from particle to particle. The internal field distribution is partially the result of irregular particle shape and partially because of the random spin distribution, varying according to the large contribution of the characteristic dimension of particle size.[31] Hence, the displacement of spins becomes Δ-, D- and radius (r)-dependent when considering spherical drops. However, when Δ is sufficiently large, the maximum displacement reached is the drop size and the signal decay becomes sensitive to droplet size and geometric shape while being Δ independent.[39]

Restricted diffusion theory states that D value should be smaller than the free diffusion value because of the limitation imposed by the size of the particles. To neglect the limiting effect of particles in molecular diffusion, twice the particle radius should be much larger than the root of the mean square displacement ($2r \gg (\Delta z^2)^{1/2}$). At the limit of high r values or low Δ values, the spin echo decay returns to the free diffusion case, calculated by equation 1.[31] However, in the DSD experiments, the time Δ used should be long enough such that the root of the mean square displacement of spins is on the same order as the particle radius ($\Delta \cong r^2/2D$).[33] Hence, the echo signal attenuation ratio also becomes a function of r and D following the equation by Murday and Cotts[31] and perfected by Packer and Rees:[33]

$$K(\Delta,\delta,g,D,r) = \exp\left[-2\gamma^2 g^2 \sum_{m=1}^{\infty}\left[\alpha_m^2\left(\alpha_m^2 r^2 - 2\right)\right]^{-1} \times \left(\frac{2\delta}{\alpha_m^2 D} - \frac{2 + e^{\left[-\alpha_m^2 D(\Delta-\delta)\right]} - 2e^{\left(-\alpha_m^2 D\Delta\right)} - 2e^{\left(-\alpha_m^2 D\delta\right)} + e^{\left[-\alpha_m^2 D(\Delta+\delta)\right]}}{\left(\alpha_m^2 D\right)^2}\right)\right] \quad (2)$$

where $K(\Delta,\delta,g,D,r) = \frac{I}{I_0}$ and α_m is the n^{th} root of Bessel's equation:

$$(\alpha_m r)J'_{3/2}(\alpha_m r) - \frac{1}{2}J_{3/2}(\alpha_m r) = 0 \quad (3)$$

Packer and Rees[33] contributed to the analysis of emulsion drops by proposing the use of a radius probability distribution P(r), where the attenuation ratio of the observed echo for the case of spherical particles is:

$$K_{obs}(\Delta,g,\delta) = \frac{\int_0^{\infty} r^3 P(r) K(\Delta,\delta,g,D,r)\,dr}{\int_0^{\infty} r^3 P(r)\,dr} \quad (4)$$

where K(Δ, δ, g, D, r) is obtained by equation 2. As the algebraic form of P(r) cannot be determined by experimental data, Packer and Rees[33] chose the lognormal distribution to obtain size distribution according to the greatest representativeness of many emulsion classes. The lognormal function is presented below:

$$P(r) = \frac{1}{2r\sigma(2\pi)^{1/2}} e^{\left[-\frac{(\ln 2r - \ln d_m)^2}{2\sigma^2}\right]} \quad (5)$$

where d_m is the median of diameters and σ is the range of standard deviation of the distribution.

For measuring the emulsion DSDs, the pulse sequence applied here (Figure 2), known as DROPTRIG, is similar to PFGSTE, but adds an initial 180° pulse, which performs a T_1 (longitudinal relaxation time) filter and eliminates the continuous phase signal by selecting "tau null" value (τ_{null}). Additionally, a secondary magnetic

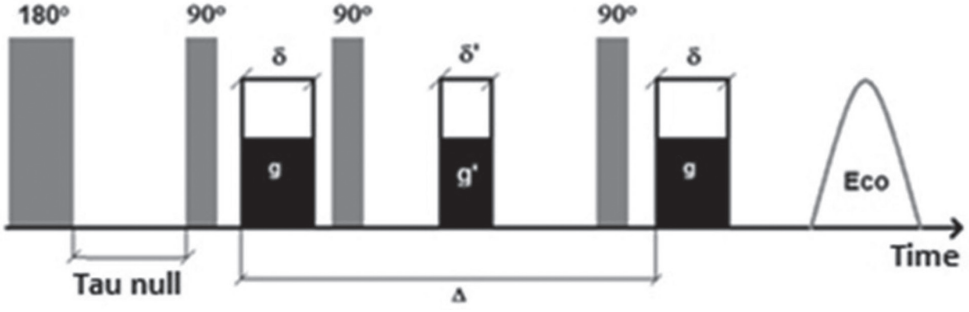

Figure 2. DROPTRIG pulse sequences.

field-gradient pulse (G') between the second and third 90° pulses "cleanses" the transversal magnetization. Therefore, only water droplet signals will be recovered in the case of W/O emulsions.

As discussed by Fridjonsson *et al.*,[37] the crude oil phase is a very complex multi-component system and there is a distribution of T_1, making it very hard to choose the best value of τ_{null}. Additionally, by changing the oil phase, τ_{null} change as well, and it must be found at a fixed temperature as it influences the dynamic emulsion processes and molecular diffusion. Another important parameter is the Δ, and it should be chosen to allow molecular displacement within the drop to reach the order of its radius, thus avoiding a low signal/noise ratio owing to relaxation processes, especially in very large drops. Van Den Enden *et al.*[15] showed that the effect of temperature on the attenuation of spin echoes is practically independent of the increase in the Δ value at 5 °C, but at 25 °C, this attenuation rises significantly with increasing Δ value at different extensions for varied samples.

The DROPTRIG sequence was applied to find the best τ_{null} value, calibrate the gradient pulse amplitude and determine the diffusion coefficient value of the pure dispersed phase as well as the DSD of the emulsion following the Murday and Cotts[31] model. The steps performed are described in the "NMR measurements" sub-section.

Materials

The two Brazilian crude oils (1 and 2) used to prepare the emulsions are classified as heavy and medium, respectively, according to National Agency of Oil, Gas and Biofuels (ANP, Agência Nacional de Petróleo, Gás e Biocombustíveis).[40] Its properties are listed in Table 1 and, at first, 10 g L^{-1} NaCl solution was used as the dispersed phase.

Emulsions preparation

Water/oil emulsions were prepared by placing the oil in a plastic container 7 cm high and 8 cm in diameter, then the dispersed phase was introduced seeking a total mass of 50 g. The Ultra Turrax T25 Digital homogenizer was used to mix the phases immediately before each analysis. During the shear process, the plastic container was slowly moved in all directions. The 28 emulsions with oils 1 and 2 were prepared by varying the dispersed phase content ranging from 1.5 to 30 wt.%, shear rate of 1000 to 6000 rpm and shear time of 1 to 6 min. Initially, 10 g L^{-1} NaCl solution was taken as dispersed phase with oils 1 and 2. Thereafter, production water was mixed with oil 1 to simulate real emulsions.

Stability test

Emulsion stability was assessed before initiating the measurements using the low-angle laser light scattering (LALLS) technique to ensure that there would be no change during DSD analysis. For this, two emulsions with 30 wt.% of NaCl solution content was prepared with oils 1 and 2. The stability test was conducted via three measurements in each emulsion. The first of them was made immediately after the preparation, the second after 1 h and the third after 2 h. No change in DSDs was observed, therefore indicating great stability of emulsions during that period. This is important considering the high complexity of the system, which can make the measurements take place for a long time in terms of appreciable signal acquisition.

Laser-scattering measurements

For emulsion stability and comparison with the NMR measurement tests, the MasterSizer MICRO MAF 5000 particle size analyzer (Malvern Instruments®) was used. This equipment can measure particles with size ranging from 0.3 to 300 μm depending of the system analyzed. It is important to note that the sensitivity of the equipment is quite limited at the extremes of this range. It is controlled by a computer with appropriated software for acquisition of statistical signs and treatment[46] and operates according to Mie's theory.[47] The analysis is done by statistical estimation as the fluid travels through the equipment. In the case of W/O emulsions, the open cycle was used to avoid interferences caused by air

Table 1. Crude oil properties

Property	Oil 1	Oil 2	Method
API gravity	20.7	29.4	ISO 12185[41]
Kinematic viscosity at 20 °C / (mm^2 s^{-1})	369.63	31.95	ASTM D7042[42]
Density at 20 °C / (g cm^{-3})	0.9262	0.8757	ASTM D5002[43]
Total acidic number / (mg KOH g^{-1} of oil)	0.506	0.096	ASTM D664[44]
Water content / (% v/v)	0.4	2.0	ASTM D4377[45]

API: American Petroleum Institute.

bubbles that may be introduced during the fluid pumping. This instrument applies the LALLS technique, generically known as "light scattering", which consists of measuring the diffraction angle of the laser radius when it interacts with a particle, which in turn are related to the particle size. The reproducibility of the results is made by the integration of several individuals averages and allows the easy verification of the calibration through standard materials,[48] such that larger particles scatter light to lower angles. The laser used has a fixed wavelength of 0.63 μm and detectors for light scattering, which send messages to a computer that calculates and provides the results.

For analysis, it was used approximately 450 mL of dispersant, which consists of a mineral oil (pharmaceutical-grade vaseline; Vitória Produtos Ltda.) and *n*-heptane (Vetec Química Fina) mixture of 7:3 ratio. The dispersant was used to calibrate the apparatus, and it was prepared one day before each analysis with vacuum filtration to remove solids particles up to 0.5 μm and left to rest to remove bubble gas particles. Neutral detergent and a specific detergent (Deterc, alkaline range) with pH between 9.5 and 10.5 (Vetec Química Fina) were used to clean the lens. The refractive index for the emulsions changed from 1.330 (water) to 1.465 (W/O emulsions). In that case, the refractive index to oils was 1.530 and for the dispersant (vaseline/heptane) was equal to 1.448. The propellers were adjusted to 2500 rpm and just a few droplets of the emulsions were used in all experiments.

The distribution results provided by the equipment include statistical parameters of distribution curve and sizes, such as median, mean volumetric diameter, among others. In this study, the droplet size distribution curve and the volumetric diameter D(4.3) measured were selected for the purpose of evaluating the emulsions. In particular, the parameter D(4.3) corresponds to the diameter of the sphere that has the same volume as the constituent particles of the system.

NMR measurements

The experiments were performed using a Maran Ultra-2 spectrometer by Oxford Instruments Molecular Biotools Ltd., which operates in a 52 mT magnetic field, corresponding to a frequency of 2.2 MHz for the ^{1}H nucleus. The instrument was calibrated with approximately 25 g of distilled water after 10 min of thermal stabilization inside the NMR. After calibration, the CPMG (Carr-Purcell-Meiboom-Gill) sequence was also used to measure the transverse relaxation time (T_2) of the water and oils. The following parameters were used: 90° and 180° pulse durations of 8.3 and 16.6 μs, respectively; number of scans (NS) of 4; number of echoes (NECH) of 32768; recycle delay (RD) 15 s; and and time between successive rephasing pulses (TAU) 200 μs. With the CPMG results, the program WinDXP® was used to obtain the T_2 distribution curve by applying the inverse Laplace transform.

To measure DSD with the DROPTRIG sequence, the following steps were performed:

(*i*) Suppression of the continuous phase signal with approximately 25 g of oil that was placed in the probe for approximately 10 min to reach thermal equilibrium at 27.5 °C. Various independent experiments were performed using the DROPTRIG sequence, varying only the τ_{null} value and holding all other parameters constant. In this experiment, oil 2 had the highest τ_{null} (110 ms), while oil 1 had τ_{null} values between 30 and 50 ms.

Table 2. Parameters used for the different liquids

Parameter	Distilled H_2O	10 g L^{-1} NaCl solution	Dehydrated oil	Emulsion
D1 / μs	100	100	100	100
D2 / μs	8000	8000	6000	6000-15000
D3 (δ) / μs	500-4500	500-4500	500-4500	500-13000
D4 (Δ) / μs	100000	100000	50000-100000	30000-100000
D5 (δ') / μs	1000	1000	1000	1000
SI	256	256	256	256
NS	4	4	16-64	16-64
RD / s	10	10	4	5
RG	10	10	10	10
G1(g)	6000	6000	25000	25000
τ_{Null} / ms	50	50	30-110	30-110

D1: pre gradient delay; D2: time between the first two pulse 90 degrees; D3 (δ): duration of the gradient pulse; D4 (Δ): time between the two gradient pulses; D5 (δ'): duration of the secondary gradient pulse; SI: size of acquisition; NS: number of scans; RD: relaxation delay; RG: receiver gain; G1(g): strength of the gradient pulses; τ_{Null}: time used to suppress the sign of the continuous phase.

(*ii*) Gradient intensity was calibrated with a list of gradient-pulse duration (δ) values summarized in Table 2.

(*iii*) Same procedure described in (*ii*) was applied to determine the diffusion coefficient for the pure dispersion phase.

(*iv*) Emulsions prepared were analyzed after 10 min to reach thermal equilibrium at 27.5 °C. The analyses were performed in duplicate using more than half of the emulsion prepared. The used parameters are presented in Table 2 with the other phases measured in the previous steps.

The values described act as starting points for oil emulsions synthesized under the same conditions, but the adjustments should be performed according to the instrument and emulsion studied. The δ list used, for instance, is strongly dependent on the system studied and varies when other parameters are altered. In some emulsions used, a list of 500-2500 μs was enough, and for others, it was necessary to use 500-13000 μs with eight linearly spaced points to attenuate the signal.

The post-processing provides two droplet size distributions, one in red for mean size, and one blue that represents the mean size distribution weighted by droplet volume. The blue distribution can provide important information on food emulsion area. Therefore, here we consider just the red curve because it is more relevant to the oil industry.

Results and Discussion

The DROPTRIG pulse sequence applied in this paper functions by suppressing the continuous phase signal for acquisition of the dispersed phase signal. This is a critical part of the analysis and requires a correct choice of τ_{null} value. Figure 3 shows how the DROPTRIG sequence was capable of correctly eliminating the continuous phase signal from oil 1 and its emulsions with different dispersed phase content, even performing measurements in systems with very low dispersed phase content (S10 with 1.51 wt.%), suggesting reliable sensibility. As expected, the sample signal increased with increasing dispersed phase content. The similar intensity of S7 (21.40 wt.%) and S8 (5.03 wt.%) emulsions is attributed to the large amount of the S8 emulsion transferred to the analysis tube.

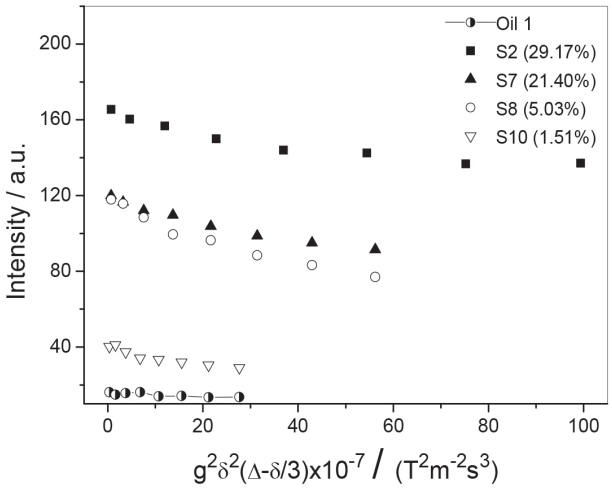

Figure 3. Signal separation of oil 1 and the emulsions with different dispersion phase contents. The list used for sample S2 was of 500-6000 μs, whereas for the other emulsions, a list of 500-4500 μs was employed. However, the Δ and τ_{null} values for S10 were from 100000 to 50000 μs.

Table 3 lists the mean values of the triplicate analysis of the S1 to S10 emulsions. All median of the mean radial values (R_{00}) and medians (R_0) of the different distributions are seen. It was expected that the S3 emulsion had the lowest average radius value because the highest shear rate (6000 rpm) was used to prepare it, and S1 had the highest R_{00} value owing to the lower applied shear rate. However, R_{00} values were in a narrow range between

Table 3. Mean radius (R_{00}) and median radius (R_0) of oil 1 emulsions obtained for different contents of the dispersion phase and shearing conditions

Emulsion	R_{00} / μm	R_0 / μm	R_{33} / μm	Std / μm	Disperse phase / wt.%	V / rpm	t / min
S1	1.180	0.920	5.620	0.970	29.69	1000	3
S2	1.380	1.365	1.447	0.147	29.17	3000	3
S3	1.384	1.381	1.402	0.091	27.06	6000	3
S4	0.835	0.428	46.166	1.400	29.87	3000	1
S5	1.235	1.235	1.235	0.003	30.03	3000	6
S6	1.681	1.678	1.705	0.096	21.40	3000	3
S7	1.678	1.677	1.680	0.032	18.31	3000	3
S8	1.750	1.734	1.857	0.179	5.03	3000	3
S9	1.640	1.614	1.818	0.202	3.34	3000	3
S10	1.661	1.652	1.718	0.130	1.51	3000	3

R_{00}: median of the mean radial values; R_0: median of the median radial values; R_{33}: median of the radius volume weighted mean; Std: standard deviation; V: shear rate; t: shear time.

0.835 and 1.750 μm, indicating that shear conditions were quite severe and variations in dispersed phase content as well as shear conditions did not significantly change the droplet size.

DSD is a more informative parameter of the system's real behavior. Comparing the representative distributions of the S1 (Figure 4a), S2 (Figure 4b) and S3 (Figure 4c) emulsions, we can see that increasing the shear rate from 1000 to 6000 rpm led to the production of finer distributions, which means more homogeneous droplets. Considering S2 (Figure 4b) and S4 (Figure 4d) emulsions, a larger distribution can be observed because of the short shear time. The smaller droplet size in the S4 emulsion was not expected and can be attributed to non-ideal behavior of the Turrax homogenizer, but still corroborates with the small droplet sizes. Observing S1 (Figure 4a) and S4 (Figure 4d) emulsions, prepared at 1000 rpm for 3 min and 3000 rpm for 1 min, respectively, we can see that the increase in the shear rate provided smaller droplets with larger distributions. All results were consistent. Furthermore, S3 and S5 (Figure not shown) emulsions are very similar and both can be represented by the distribution (Figure 4c). Finally, the Figure 4b distribution can represent S6 to S10 emulsions (Figures not shown) because of the same shear conditions used. It is noteworthy that each analysis was performed in approximately 15 min, a great result that allows the application of this technique in routine analyses.

The distributions in Figure 4 shows good agreement with those obtained by Fridjonsson *et al.*,[37] where droplets had radius ranging from less than 1 μm to about 10 μm with density between 0.82 and 0.90 g mL^{-1} for the oils and dispersed phase content ranging from 5 to 20%. The results also showed that the distributions had little variation with an increasing concentration of the aqueous phase, only slightly shifting the distribution to larger sizes and corroborating with the results of the present article.

To validate the NMR results, similar emulsions to those in Table 3 were prepared and analyzed by the laser-scattering technique. Table 4 shows the mean values (D(4.3) and D_{00}) and the median (D(0.5) and D_0) of the diameters obtained by both techniques (laser and NMR, respectively), where the highest values were 3.50 and 1.81 μm for D_{00} and D(4.3), respectively, and 3.46 and 1.49 μm for D_0 and D(0.5), respectively.

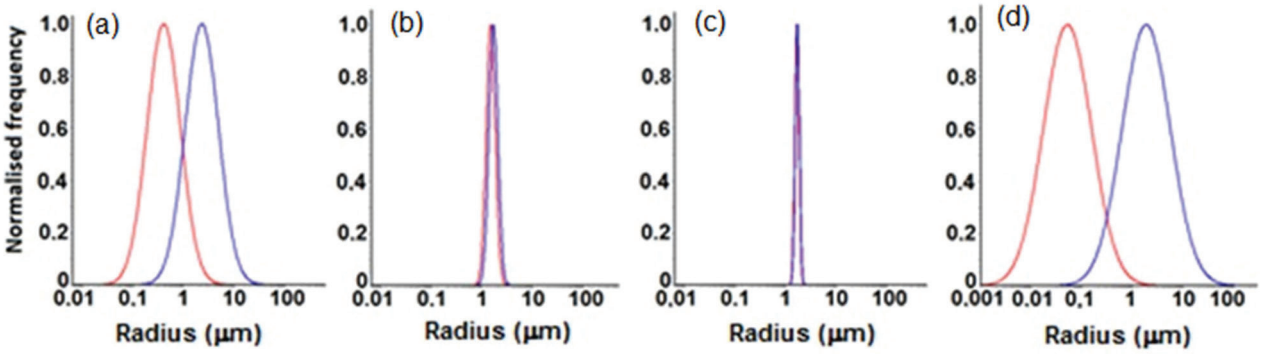

Figure 4. Droplet distribution size of (a) S1; (b) S2; (c) S3 and (d) S4 oil 1 emulsions.

Table 4. Mean and median diameters obtained by laser scattering and NMR with similar percentages and the same shearing conditions for the oil 1 emulsions

NMR			Laser		
Emulsion	D_{00} / μm	D_0 / μm	Emulsion	D(4.3) / μm	D(0.5) / μm
S1	2.36	1.84	S11	1.69	0.95
S2	2.76	2.74	S12	1.73	1.10
S3	2.76	2.76	S13	1.65	1.41
S4	1.68	0.86	S14	1.76	1.37
S5	2.48	2.48	S15	1.81	1.49
S6	3.36	3.36	S16	1.79	1.39
S7	3.36	3.36	S17	1.64	1.16
S8	3.50	3.46	S18	1.47	1.05
S9	3.28	3.22	S19	1.39	0.92
S10	3.32	3.30	S20	0.94	0.80

NMR: nuclear magnetic resonance; D_{00}: median of the mean diameters values by NMR; D_0: median of the median diameters values by NMR; D(4.3): median of the mean diameters values by laser; D(0.5): median of the medians diameters values by laser.

There are four main points to explain those differences. The first point is the unrepresentative sampling in the laser measurements, restricted to a few drops, whereas in NMR analysis a larger volume was used. The second point is the 2500 rpm value of the propeller system used to homogenize the system before the laser measurements. Although previous studies showed that this value is suitable for heavy oils emulsions, it is possible to break the droplets, mainly in lighter oil emulsions, justifying the smaller size measured by the laser equipment. The third point is the temperature effect on NMR analysis. Although coalescence was favored by the increase in temperature, the stability test showed no change in DSD for 2 h. Therefore, the droplet size increase may be negligible because of the small increase in temperature (27.5 to 30 °C). Another temperature effect is the greater diffusion of the dispersed droplets (including sedimentation or creaming processes). The drag imposed by the flow of the sample on the laser measurements governs the movement of the dispersed droplets, making the sedimentation or creaming processes negligible. However, in NMR measurements, the droplet diffusion makes the spins experience different magnetic fields between the beginning and the end of the experiment, changing both echo attenuation and droplet size measured. Van Den Enden *et al.*[15] showed that at 17.5 °C the diffusion of droplets with a radius of 0.1 μm had a negligible effect on the echo attenuation in oils with viscosity above 90 mPa s. So, it can be negligible due to the high viscosity of oil 1 (342 mPa s at 20 °C). In this case, the explanation must be related to water interdroplet diffusion, as discussed by Fourel *et al.*[49] As the droplets get close to each other agglomerating without coalescing (very common in crude oil emulsions), the passage of water molecules between different droplets occurs more easily, affecting the displacement of the molecules and, consequently, the measured size. Finally, the fourth point is that in the laser processing the mean diameter (D(4.3)) is calculated from a sphere having the same volume as the average volume of the system droplets, considering spherical droplets, while the DSD does not assume any type of distribution. In NMR measurements, as discussed by Ambrosone *et al.*,[34] the signal is also proportional to the droplet volume because the contribution of each drop in the echo attenuation is proportional to the number of spins contained in the drop. Although it also considers spherical droplets, the processing applies the lognormal distribution, resulting in different statistical means in comparison to the laser results.

Although the NMR values are higher than the laser-scattering technique, it is possible to observe a good agreement between the results obtained by the different techniques with heavy crude oil emulsions. Additionally, it is not intended in this paper to show that laser-scattering and NMR techniques lead to the same results, but to show NMR's ability to measure emulsions with different properties are in robust agreement with other techniques, as can be seen by the same information obtained through the different measures regarding the classification of emulsions and the best method of separation, presented in the Introduction section of this article.

The signal separation occurs by appropriate choice of τ_{null}, which is related to the longitudinal relaxation time and, in turn, has a strong approximation of the transversal relaxation time. It is well known in the literature[20] that there is an inverse relationship between oil viscosity and relaxation time, making clear the importance of knowing oil viscosity. However, based on the high crude oil complexity, there is no unique value for relaxation times (T_1 or T_2), but a distribution of values that can result in significant signal loss or even overlapping phase signals, making measurement impossible. To illustrate, Figure 5a (S6 emulsion) shows that the transversal relaxation time (T_2) for oil 1 was 18 ms, smaller than dispersed water (971.46 ms). Clearly, there was no overlap of the water and oil phase times, explaining the ease in signal separation of the oil 1 emulsions from the NMR point of view. On the other hand, oil 2 with lower viscosity showed T_2 = 133.30 ms, evidently, there was an overlap of the distribution of transverse relaxation times in emulsion S24, as shown in Figure 5b.

Although there is signal overlap in the second case, Figure 6 indicates that the DROPTRIG is reliable, even in that situation. Figure 6a shows the signal separation of the S21 emulsion with 30.36 wt.% dispersed phase content. As it had higher content, it was not necessary to increase the number of scans. However, in emulsions S22 to S24, it was necessary to acquire a greater amount of signal.

Figure 6a shows that there is a good signal separation of the S21 (30.36 wt.%) emulsion with 16 NS. In emulsions S22 to S24 with less than 20 wt.% dispersed phase content, 64 scans were necessary because of the loss of part of the dispersed phase signal during the elimination of the continuous phase signal. However, even with this difficulty, the DROPTRIG sequence was capable of working with low viscosity oils. As a consequence of the increased number of scans, the experimental time increased from approximately 15 to roughly 40 min, which is still a reasonable time compared with the laser equipment, which takes about 20 min to clean the lenses.

The NMR and laser diameters are presented in Table 5. It can be verified that the NMR values are slightly higher. This is attributed to the higher NMR temperature and delay time in adjusting the parameters for these emulsions in addition to the previous discussion about

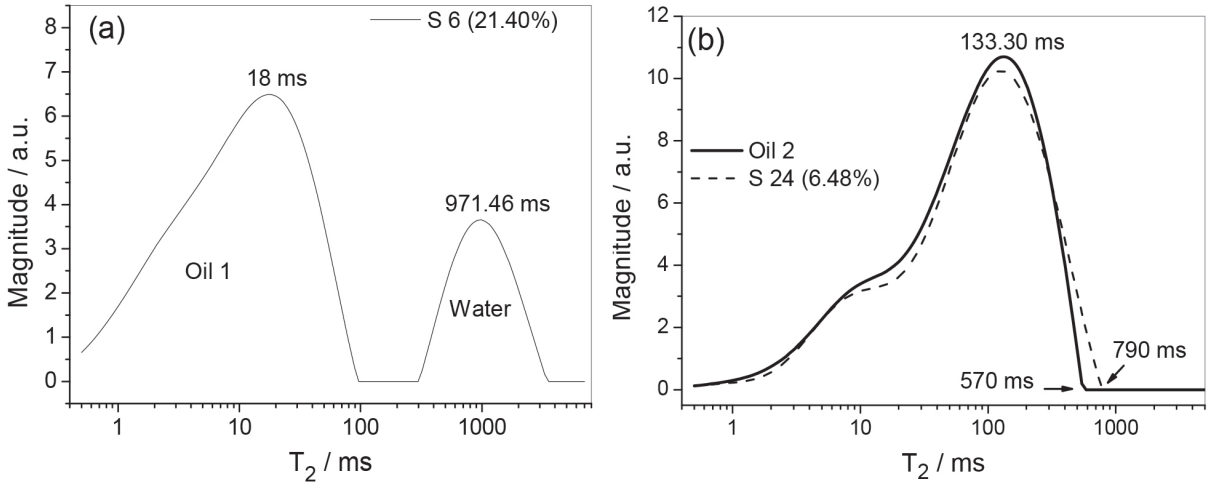

Figure 5. T_2 distribution curve of (a) S6 of oil 1 and (b) S24 of oil 2 obtained from CPMG experiment.

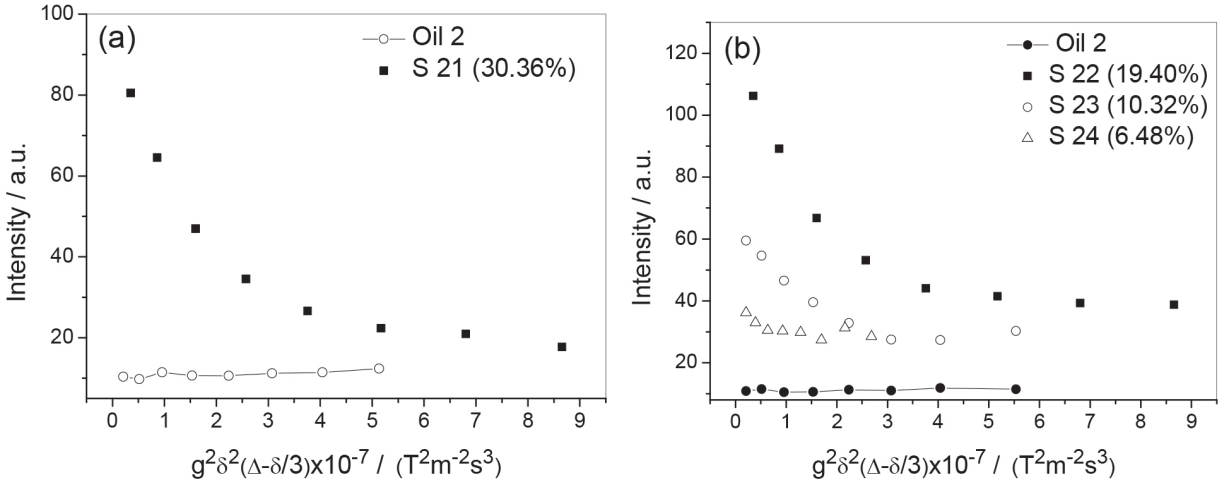

Figure 6. Decay curves indicating signal separation of oil 2 emulsions: (a) S21 with NS 16 and (b) S22 to S24 using NS 64. NS is the number of scans.

the differences between the techniques. Considering the longer experimental time (approximately 40 min), higher temperature, and because they are lighter oil emulsions (28 mPa s at 20 °C), the water droplets have greater mobility and suffer greater influence of the droplets' diffusion. In addition, the higher temperature increases the passage of the water molecules to different droplets, as previously discussed. This explains the greater difference observed in the results of oil 2 emulsions (lower viscosity) in relation to the laser results when compared with oil 1 emulsions (higher viscosity). To avoid the temperature effect on the echo attenuation, as highlighted by Van Den Enden *et al.*,[15] these measurements should be performed at 5 °C. Although the values are slightly different, there is considerable agreement of small droplet sizes in different measurements, making the results satisfactory. Finally, despite the rather apparent separation of the signal from emulsion S24, its values were disregarded in Table 5 based on problems with the data treatment.

To test the technique in a real emulsions case, four emulsions were prepared using production water, which has paramagnetic ions and can promote a faster relaxation magnetization. Figure 7 compares the pure oil 1 signal with its emulsions.

According to Figure 7, the NMR technique was capable of signal separation between the oil and water phases despite the paramagnetic ion presence. The proximity of the S26 (20.60 wt.%) and S27 (11.02 wt.%) emulsion signals have the same explanation for the S7 and S8 emulsions. The results of this analysis are shown in Table 6.

According to Table 6, the R_{00} and R_0 values, as expected, were very close to each other because the same shear conditions were applied. Additionally, there was great agreement with the small radius measured for the emulsions of oil 1 without paramagnetic ions, indicating that the technique can be applied in systems with paramagnetic ion presence, even in low dispersion phase emulsions (5.15 wt.%). Finally, the S25 to S28

Table 5. Comparison of NMR and laser scattering results for emulsions of oil 2

Emulsion	D_{00} / μm	D_0 / μm	D(4.3) / μm	D(0.5) / μm
S21	5.53	5.01	1.72	1.25
S22	4.52	4.02	1.74	1.26
S23	4.60	4.30	1.82	1.20
S24	not considered		1.79	1.17

D_{00}: median of the mean diameters values by NMR; D_0: median of the medians diameters values by NMR; D(4.3): median of the mean diameters values by laser; D(0.5): median of the median diameters values by laser.

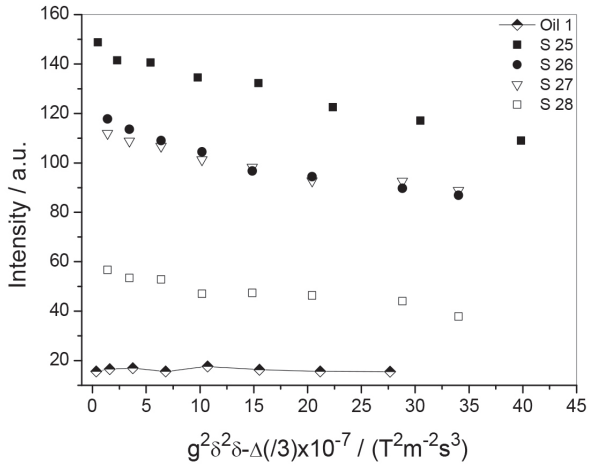

Figure 7. Separation of the oil 1 signal from the signal of emulsions simulating real systems with production water as the disperse phase.

DSDs were very similar with a small size range, as can be seen in Figure 8.

Conclusions

The results obtained by low field NMR allowed measuring DSD of W/O emulsions under different shearing conditions. DROPTRIG sequence was capable of separating the continuous and dispersion phase signals for heavy and medium oils, even with low dispersion phase content (1.51 wt.%). For emulsions prepared with production water, the mean drop radius remained very close under the same shearing conditions for dispersion phase content, ranging from 5.15 to 30.18 wt.%. In addition, it was possible to observe the effect of the shearing conditions in DSD, which always produces very small drops (D_0 and D_{00} smaller than 5.01 and 5.53 μm, respectively). The oil 2 emulsions presented greater differences in relation to the laser results than the oil 1 emulsions. Importantly, although slight differences have been observed between the different techniques because of the temperature effect in NMR measurements and different algorithms' processing, robust agreement between the NMR and laser diffraction measurements was obtained. Besides, signal separation in S24 (6.48 wt.%) was observed. Even so, emulsions with low viscosity oil continuous phase and low dispersion phase content demands further attention. Low-field NMR was effective in measuring DSD in emulsions with production

Table 6. Mean results of the real emulsions from oil 1

Emulsion	R_{00} / μm	R_0 / μm	R_{33} / μm	Std / μm	Disperse phase / wt.%	V / rpm	t / min
S25	1.484	1.480	1.513	0.118	30.18	3000	3
S26	1.484	1.471	1.568	0.201	20.60	3000	3
S27	1.351	1.305	1.659	0.289	11.02	3000	3
S28	1.486	1.452	1.701	0.319	5.15	3000	3

R_{00}: median of the mean radial values; R_0: median of the median radial values; R_{33}: median of the radius volume weighted mean; Std: standard deviation; V: shear rate; t: shear time.

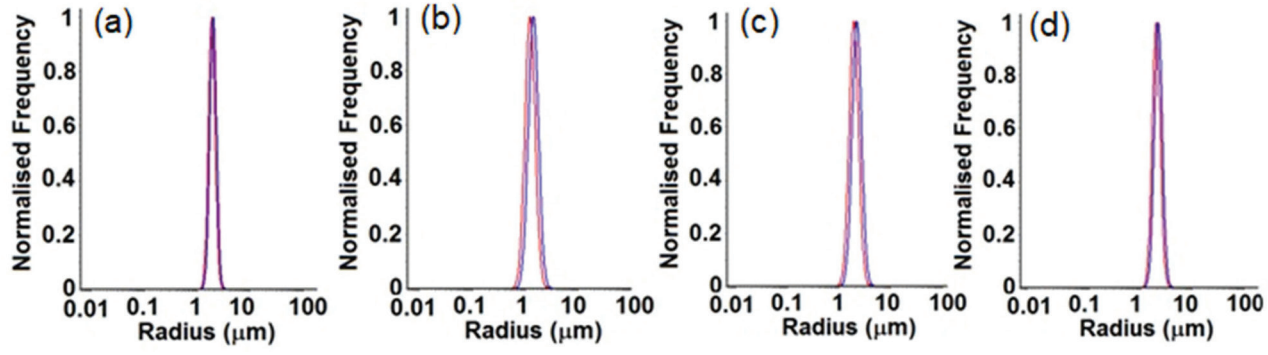

Figure 8. Droplet size distribution of the emulsions simulating real systems with oil 1 by DROPTRIG sequence: (a) S25; (b) S26; (c) S27 and (d) S28.

water. This is a great advancement for very low-field equipment, showing that it can be applied to real emulsions with good reliability and experimental times varying from 15 to 40 min. Finally, the results can contribute to a better understanding of the behavior of DSD in crude oil emulsions under different shear conditions, volumetric fractions and paramagnetic ion presence.

Acknowledgments

The authors would like to acknowledge FAPES (Fundação de Amparo à Pesquisa e Inovação do Espírito Santo), CAPES (Coordenação de Aperfeiçoamento Pessoal de Nível Superior), CNPq (Conselho Nacional de Desenvolvimento Científico e Tecnológico), NCQP (Núcleo de Competências em Química do Petróleo) for their financial and technical support and FAPESP (Fundação de Amparo à Pesquisa do Estado de São Paulo, process No. 2017/02856-0).

References

1. Kang, W.; Xu, B.; Wang, Y.; Li, Y.; Shan, X.; An, F.; Liu, J.; *Colloids Surf., A* **2011**, *384*, 555.
2. McLean, J. D.; Kilpatrick, P. K.; *J. Colloid Interface Sci.* **1997**, *189*, 242.
3. Khadim, M. A.; Sarbar, M. A.; *J. Pet. Sci. Eng.* **1999**, *23*, 213.
4. Peña, A. A.; Hirasaki, G. J.; Miller, C. A.; *Ind. Eng. Chem. Res.* **2005**, *44*, 1139.
5. Abdulbari, H. A.; Abdurahman, N. H.; Rosli, Y. M.; Mahmood, W. K.; Azhari, H. N.; *Int. J. Phys. Sci.* **2011**, *6*, 5376.
6. Opedal, N. V. D. T.; Sørland, G.; Sjöblom, J.; *Energy Fuels* **2010**, *24*, 3628.
7. Kokal, S. L. In *SPE Annual Technical Conference and Exhibition*; Society of Petroleum Engineers: San Antonio, 2002, 533, SPE 77497.
8. Farah, M. A.; Oliveira, R. C.; Caldas, J. N.; Rajagopal, K.; *J. Pet. Sci. Eng.* **2005**, *48*, 169.
9. Chanamai, R.; McClements, D. J.; *Colloids Surf., A* **2000**, *172*, 79.
10. Desnoyer, C.; Masbernat, O.; Gourdon, G.; *Chem. Eng. Sci.* **2003**, *58*, 1353.
11. https://engenhariaquimica.files.wordpress.com/2010/04/apostila-ppp.pdf, accessed in March 2019.
12. Jafari, S. M.; Assadpoor, E.; He, Y.; Bhandari, B.; *Food Hydrocolloids* **2008**, *22*, 1191.
13. Boxall, J. A.; Koh, C. A.; Sloan, E. D.; Sum, A. K.; Wu, D. T.; *Ind. Eng. Chem. Res.* **2010**, *49*, 1412.
14. Hollingsworth, K. G.; Sederman, A. J.; Buckley, C.; Gladden, L. F.; Johns, M. L.; *J. Colloid Interface Sci.* **2004**, *274*, 244.
15. Van Den Enden, J. C.; Waddington, D.; Van Aalst, H.; Van Kralingen, C. G.; Packer, K. J.; *J. Colloid Interface Sci.* **1990**, *140*, 105.
16. Flaum, M.; Hirasaki, G. J.; Flaum, C.; Straley, C.; *Magn. Reson. Imaging* **2005**, *23*, 337.
17. Fleury, M.; Deflandre F.; Godefroy, S.; *C. R. Acad. Sci., Ser. IIc: Chim.* **2001**, *4*, 869.
18. Guan, H.; Brougham, D.; Sorbie, K. S.; Packer, K. J. J.; *Pet. Sci. Eng.* **2002**, *34*, 35.
19. Fantazzini, P.; *Magn. Reson. Imaging* **2005**, *23*, 125.
20. Morgan, V. G.; Barbosa, L. L.; Lacerda Jr., V.; de Castro, E. V. R.; *Ind. Eng. Chem. Res.* **2014**, *53*, 8881.
21. Bryan, J.; Kantzas, A.; Bellehumeur, C.; *SPE Reservoir Eval. Eng.* **2005**, *8*, 44.
22. Kantzas, A.; *J. Can. Pet. Technol.* **2009**, *48*, 15.
23. Barbosa, L. L.; Kock, F. V. C.; Silva, R. C.; Freitas, J. C. C.; Lacerda Jr., V.; Castro, E. V. R.; *Energy Fuels* **2013**, *27*, 673.
24. Silva, R. C.; Carneiro, G. F.; Barbosa, L. L.; Lacerda, V.; Freitas, J. C. C.; Castro, E. V. R.; *Magn. Reson. Chem.* **2012**, *50*, 85.
25. Balinov, B.; Urdahl, O.; Söderman, O.; Sjöblom. J.; *Colloids Surf., A* **1994**, *82*, 173.
26. Peña, A. A.; Hirasaki, G. J.; *Adv. Colloid Interface Sci.* **2003**, *105*, 103.
27. Aichele, C. P.; Flaum, M.; Jiang, T.; Hirasaki, G. J.; Chapman, W. G.; *J. Colloid Interface Sci.* **2007**, *315*, 607.
28. Opedal, N. V. D. T.; Sørland, G.; Sjöblom, J.; *Diffus. Fundam.* **2009**, *7*, 1, available at http://ul.qucosa.de/api/qucosa%3A14145/attachment/ATT-0/, accessed in March 2019.
29. Sørland, G. H.; Keleşoğlu, S.; Simon, S.; Sjöblom, J.; *Diffus. Fundam.* **2013**, *19*, 1, available at http://ul.qucosa.de/api/qucosa%3A13703/attachment/ATT-0/, accessed in March 2019.
30. Tanner, J. E. J.; *J. Chem. Phys.* **1970**, *52*, 2523.
31. Murday, J. S.; Cotts, R. M.; *J. Chem. Phys.* **1968**, *48*, 4938.
32. Neuman, C. H.; *J. Chem. Phys.* **1974**, *60*, 4508.
33. Packer, K. J.; Rees, C.; *J. Colloid Interface Sci.* **1972**, *40*, 206.
34. Ambrosone, L.; Ceglie, A.; Colafemmina, G.; Palazzo, G.; *J. Chem. Phys.* **1997**, *107*, 10756.
35. Stejskal, E. O.; Tanner, J. E.; *J. Chem. Phys.* **1965**, *42*, 288.
36. Hollingsworth, K. G.; Johns, M. L.; *J. Colloid Interface Sci.* **2003**, *258*, 383.
37. Fridjonsson, E. O.; Graham, B. F.; Akhfash, M.; May, E. F.; Johns, M. L.; *Energy Fuels* **2014**, *28*, 1756.
38. Dunynhoven, J. P. M.; Goudappel, G. J. W.; Dalen, G.; Bryggen, P. C.; Blonk, J. C. G.; Eijkelenboom, A. P. A. M.; *Magn. Reson. Chem.* **2002**, *40*, 51.
39. https://www.osti.gov/servlets/purl/881436, accessed in March 2019.
40. http://www.anp.gov.br/images/publicacoes/anuario-estatistico/2018/anuario_2018.pdf, accessed in April 2019.
41. ISO12185: *Crude Petroleum and Petroleum Products Determination of Density Oscillating U-Tube Method*; ISO: Geneva, Switzerland, 1996.
42. ASTM D7042: *Standard Test Method for Dynamic Viscosity and Density of Liquids by Stabinger Viscometer (and the*

Calculation of Kinematic Viscosity); ASTM International: West Conshohocken, PA, USA, 2004, DOI: 10.1520/D7042-04.

43. ASTM D5002*: Standard Test Method for Density of Crude Oils by Digital Density Analyzer*; ASTM International: West Conshohocken, PA, USA, 2016, DOI: 10.1520/D5002-16.
44. ASTM D664: *Standard Test Method for Acid Number of Petroleum Products by Potentiometric Titration*; ASTM International: West Conshohocken, PA, USA, 2017, DOI: 10.1520/D0664-17A.
45. ASTM D4377: *Standard Test Method for Water in Crude Oils by Potentiometric Karl Fischer Titration*; ASTM International: West Conshohocken, PA, USA, 2011, DOI: 10.1520/D4377-00R11.
46. Micromeritics, Sedigraph III 5120, *Micromeritics: Description, Features and Analysis Technique*, 2006.
47. Pohl, M. C.; *ASM Handbook*, vol. 7; ASM International Handbook Committee, ed.; ASM International: Russell Township, OH, USA, 1998, p. 250.
48. ISO13320: *Particle Size Analysis - Laser Diffraction Methods Part 1: General Principles*; ISO Standards Authority: Geneva, Switzerland, 1999.
49. Fourel, I.; Guillement, J. P.; Le Botlan, D.; *J. Colloid Interface Sci.* **1994**, *164*, 48.

Submitted: January 14, 2019
Published online: April 9, 2019